Article:
Li, S, Chu, F, Zhang, J et al. (2 more authors) (2020) Droplet jumping induced by coalescence of a moving droplet and a static one: Effect of initial velocity. Chemical Engineering Science, 211. 115252. ISSN 0009-2509

https://doi.org/10.1016/j.ces.2019.115252

Droplet jumping induced by coalescence of a moving droplet and a static one: Effect of initial velocity

Shaokang Li [a], Fuqiang Chu [a,*], Jun Zhang [a], Haichuan Jin [a], David Brutin [b], Dongsheng Wen [a,c,*]

[a] School of Aeronautic Science and Engineering, Beihang University, Beijing 100191, China

[b] Aix-Marseille University, IUSTI UMR CNRS 7343, Marseille, France

[c] School of Chemical and Process Engineering, University of Leeds, Leeds LS2 9JT, UK

*Corresponding authors. E-mail addresses: chufq18@buaa.edu.cn (F. Chu), d.wen@buaa.edu.cn (D. Wen)

Abstract

The phenomenon of coalescence-induced droplet jumping on superhydrophobic surfaces has a wide range of applications such as hotspot cooling, surface self-cleaning, anti-icing, and defrosting. Previous experimental and numerical studies mainly focused on the coalescence of static droplets with varying droplet properties and substrate structures. However, in practice, it is more common to see a moving droplet hit a stationary one, which leads to a coalesced droplet jumping from the surface. To explore the effect of initial velocity on the jumping behavior of coalesced droplet, we performed simulations using the volume of fluid method with a dynamic contact angle model, and validated the simulation results against our experiments. We analyzed the morphology evolutions, velocity variations and energy conversion rates during the jumping process. The results show that the initial velocity of the moving droplet accelerates the droplet deformation during jumping, resulting in a unique departure feature. Droplet departs at different stages under different initial velocities, and the departure velocity is approximately constant at the first stage and then increases with increasing initial velocity. The variation in energy conversion rate is consistent with the departure velocity which suggests the conversion rate has a slight change in low initial velocity range. This work shall bring new insights into the droplet jumping regulation and promote the application of droplet jumping in related fields.

Keywords: droplet jumping; initial velocity; morphology; departure velocity; energy conversion rate

1. Introduction

When condensation occurs on the superhydrophobic surface, merged droplet can jump from the surface, which called the droplet jumping phenomenon. This phenomenon was first reported by Boreyko and Chen in 2009,[1] and following that, many experimental observations [2-7] and numerical simulations [8-14] have been reported. Since the occurrence of droplet jumping is spontaneous which means no external energy is required, it could be applied to many applications, such as hotspot cooling, self-cleaning, heat transfer enhancement, anti-icing and defrosting.[15-26]

Coalescence-induced droplets jumping is triggered by the surface energy released during the merging process, and the dynamics of the coalescent droplet is governed by an equilibrium balance of surface energy, kinetic energy, and the viscous dissipation.[12, 27] In actual situation, the viscous dissipation inside the droplet, as well as the work of adhesion between the droplet and the surface, blocks the movement of coalescent droplet which causes only a small part of excess surface energy converting into jumping kinetic energy.[8] Jumping velocity is an important parameter that represents dynamic characteristics in the process. Lecointre *et al.* and Mouterde *et al.* gave a modified equation

for jumping velocity as, [28, 29]

$$v_{depar} \approx \frac{u_{ci}}{4}[\alpha - 4Oh] \quad (1)$$

where u_{ci} is the capillary-inertia velocity, *i.e.*, $u_{ci}=(\sigma/\rho_l r_0)^{1/2}$, σ is water surface tension, ρ_l is water density, r_0 is the droplet radius; *Oh* is the Ohnesorge number that can be written as $Oh=\eta_l/(\rho_l\sigma r_0)^{1/2}$, η_l is the viscosity of water; α is a numerical coefficient close to unity at large surface contact angle; and v_{depar} is the velocity at which the droplet leaves the surface.

In addition to the above studies, many influencing factors on the jumping phenomenon have been investigated such as the droplet itself and surface properties, leading to different droplet morphology, jumping velocity, and energy conversion characteristics. For coalescence-induced jumping of two equal-sized droplets, Cheng *et al*. [12, 13] developed 2D and 3D Lattice Boltzmann methods (LBM) and established a relationship between droplet jumping velocity and droplet radius. Liu *et al*. [8, 30] investigated the mechanism of self-propelled jumping on a non-wetting surface by both experimental and numerical methods. The whole process was divided into four stages and the trend of jumping velocity under different *Oh* numbers was analyzed. Nam *et al*. [31] reported changes in various energies for droplet jumping with a full 3D numerical model supported by experiment results. Their results showed that half of the released surface energy could transfer into the kinetic energy before droplet departure. Based on the results about equal size droplets, research on droplets with different radii ratios is also constantly evolving. Mouterde *et al.* [28] investigated the jumping velocity both symmetric and asymmetric coalescence in experiments, proposing that the jumping velocity of asymmetric coalescence depended on the smaller droplets. Exploiting that finding, the takeoff velocity was predicted quantitatively in the case of ignoring adhesion. Wang *et al*. [32] focused on the effects of the initial droplet size radio. For the size range of the larger droplet is between 1 μm to 100 μm, droplet jumping does not occur when the radius ratio is less than 0.56. Wasserfall *et al.* [33] investigated the effects of droplet radio, viscosity and contact angle on the jumping process induced by unequal-sized droplet merging. Multidroplet-coalescence induced jumping has also been studied. Chu *et al*. [34] studied the influences about the number of droplets and the arrangement of three droplets. The variation tendency of surface energy and velocity under different conditions as well as the energy conversion rate were obtained. Wang *et al.* [35] studied the jumping of three droplets, and set two arrangements: (i) three droplets in contact with each other in initial, and (ii) two droplets are in contact initially and are in contact with the third droplet during the merging process.

Besides these discussions about droplet size and number, surface property is also an important factor affecting the jumping behavior. Cheng *et al*. [13] used a 3D Lattice Boltzmann method to investigate the effects of textured surface, and proposed that there was an optimum spacing of the microstructures for the maximum jumping velocity.

Attarzadeh *et al.* [36] used the volume of fluid (VOF) method to simulate the effects of heterogeneous surface on this phenomenon and showed that the heterogeneous surface increased the adhesion of the droplets and reduced the jumping velocity and jumping height. Designing special structures to enhance jumping is also a hot topic in this field. Both Wang *et al*. [37] and Vahabi *et al.* [38] set ridges between two droplets on a smooth superhydrophobic surface, and concluded that the droplet jumping height as well as the energy conversion rate increased significantly comparing with jumping on a superhydrophobic surface without a ridge.

It shall be noted that all these studies were about static droplets. As for moving droplets, Liu *et al.* [30] and Chen *et al.* [10] studied a process of two-droplet-coalescence-jumping with the same approaching velocity, and showed that the takeoff speed remained constant when the approach velocities were low, but the takeoff speed increased significantly after the velocity greater than 1 m/s. However, in the process of condensation, it is more common to see a moving droplet impact on another stationary droplet at a certain initial velocity, resulting in a jumping phenomenon from the surface. It appears that controlling the initial velocity of moving droplets could be used to regulate the movement of droplets. In this work, detailed droplet jumping phenomenon induced by the coalescence of a moving droplet and a static one is studied numerically by the VOF method to understand the effects of the initial velocity of the moving droplet, which could be of fundamental interest to a number of applications.

2. Methodology

2.1 Numerical model

In this work, we employed interFoam solver in Open Source Field Operation and Manipulation (OpenFOAM) C++ libraries [39] to perform numerical simulations. This solver assigns a volume fraction (φ) in each computation cell to capture the interface,[40-42] the volume fraction (φ) has a value range of 0-1 (φ=0 represents the gas phase, φ=1 represents the liquid phase, and $0<\varphi<1$ corresponds to the interface area). The fluid properties, such as the weighted-average density and viscosity in each cell can be expressed as,

$$\rho = \varphi\rho_{\mathrm{l}} + (1-\varphi)\rho_{\mathrm{g}} \quad (2)$$

$$\eta = \varphi\eta_{\mathrm{l}} + (1-\varphi)\eta_{\mathrm{g}} \quad (3)$$

The governing equations within interFoam solver for the continuity and momentum equations are shown as following.

$$\frac{\partial\rho}{\partial \mathrm{t}} + \nabla(\rho \times \mathrm{U}) = 0 \quad (4)$$

$$\frac{\partial}{\partial \mathrm{t}}(\rho \mathrm{U}) + \nabla(\rho \mathrm{U} \otimes \mathrm{U}) = \nabla\tau - \nabla \mathrm{p} + \mathrm{f} \quad (5)$$

where U is the velocity vector, t is the time, p is the pressure, τ is the viscous stress tensor. f is the surface tension

force and can be calculated following the continuum surface force (CSF) model,

$$\mathrm{f} = \sigma\kappa\nabla\varphi \quad (6)$$

where σ is the surface tension and κ is the mean curvature of the free surface,

$$\kappa = -\nabla\cdot\left(\frac{\nabla\varphi}{|\nabla\varphi|}\right) \quad (7)$$

For continuous two-phase flow with constant densities, the volume fraction φ satisfies the advection equation which can be expressed as,

$$\frac{\partial\varphi}{\partial \mathrm{t}} + \nabla\left(\varphi \otimes \mathrm{U}\right) = 0 \quad (8)$$

The dynamic contact angle is also considered with the Kistler's model selected in this simulation.[43] The algorithm will be used for every time step, the formulas are shown in the below.

$$\theta_{\mathrm{d}} = \mathrm{f_H}\left(\mathrm{Ca} + \mathrm{f_H^{-1}}\left(\theta_{\mathrm{e}}\right)\right) \quad (9)$$

where $\mathrm{f_H^{-1}}$ is the inverse function of the "Hoffman's" empirical function, the equation is shown below.

$$\mathrm{f_H} = \arccos\left\{1 - 2\tanh\left[5.16\left[\frac{\mathrm{x}}{1+1.31\mathrm{x}^{0.99}}\right]^{0.706}\right]\right\} \quad (10)$$

The Capillary number *Ca* is defined as,

$$\mathrm{Ca} = \frac{\eta \mathrm{v_{cl}}}{\sigma} \quad (11)$$

where v_{cl} is the velocity of contact line.

In the equation, the dynamic contact angle is related to the velocity of contact line.[44, 45] We modified the interFoam solver that added the dynamic contact angle as a boundary condition into it.[46] During the simulation, the value of advancing contact angle and receding contact angle are set according to the surface properties.

2.2 Computational domain and dimensionless analysis

Figure 1(a) is the schematic of the droplet jumping induced by coalescence of a moving droplet and a static one that we investigated in this work. Left droplet with an initial velocity moves to the right droplet then jumps together in the oblique direction. Figure 1(b) is the 3D simulation model of the process. To save computation resources, we placed the two droplets contact with each other in the beginning and set a determined velocity on the left droplet to investigate the influences of the initial velocity. In Fig. 1(b), the size of computation domain is 1.5 mm × 1.5 mm × 1.5 mm, and the radius of droplet is 150 μm. The bottom surface is set as a no-slip wall with the other boundaries as pressure outlet boundaries.[8, 11, 34] The distance between droplets and the surrounding boundary is large enough which ensures the pressure boundaries have a minimal effect for the process. The equilibrium contact

angle of the bottom surface, θ, is 160° with a dynamic contact angle of ±5°, which means the advancing contact angle, θ_A, is 165° and receding contact angle, θ_R, is 155°. In this simulation, we chose the physical properties of the water droplet and gas at 20℃ (shown in Table 1) to calculate the fluid properties.

Table 1. Physical properties of water and gas at 20℃

σ（N/m）	ρ_l (kg/m^3)	η_l (Pa s)	ρ_g(kg/m^3)	η_g (Pa s)
0.07275	998	0.001005	1.293	1.8×10^{-5}

For the case that the initial droplet velocity is 0.5 m/s, we set up four kinds of meshes, whose mesh densities are 100×100×100, 150×150×150, 200×200×200, and 250×250×250, to do the grid independence verification. Every time we increased the mesh density, we compared the relative changes of the vertical velocity curves (u_{jump}) before the droplet departure. The results show that, when the mesh density is increased from 100×100×100 to 150×150×150, the vertical velocity changes 14.2%, while the changes are 3.8% and 3.7% when the mesh densities are increased from 150×150×150 to 200×200×200 and from 200×200×200 to 250×250×250, respectively. Thus, to save computing resources while ensuring computational accuracy, we chose the 150×150×150 mesh for calculation.

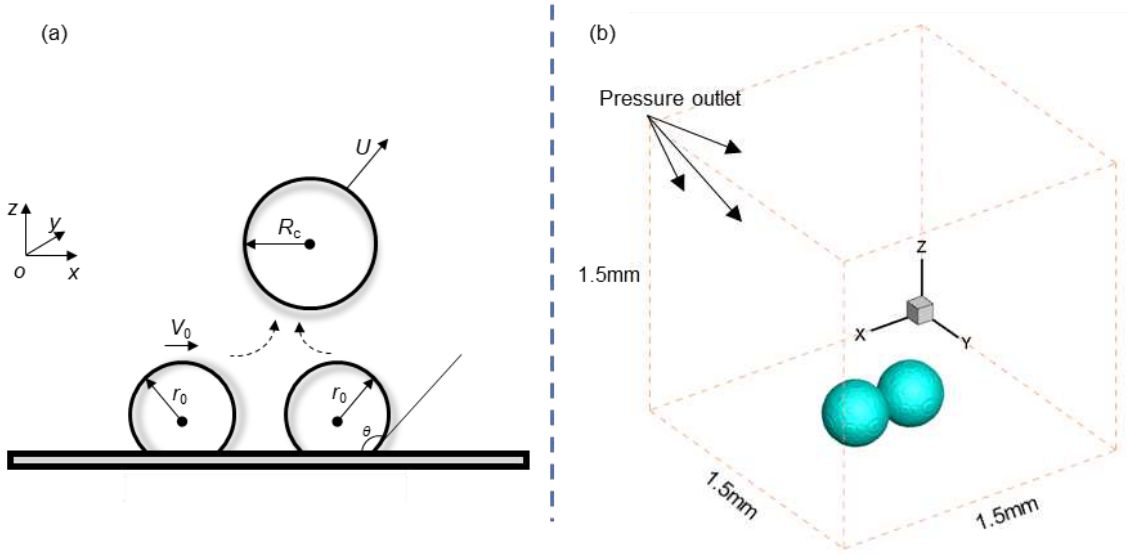

Fig. 1. (a) Schematic diagram of droplet jumping induced by coalescence of a moving droplet and a static one. The left droplet has a velocity which moves toward the stationary droplet and then they jump together after merge on the superhydrophobic surface. (b) 3D model of the simulation. At initial time, two droplets contact with each other. We set an initial velocity on the left droplet.

Since the left droplet is exerted with velocity, we focus on the vertical velocity u_{jump} and the horizontal velocity u_x throughout the jumping process, where the two velocities are calculated as the mass-average velocity.

$$u_{jump} = \frac{\int_V \rho_l w dV}{\int_V \rho_l dV} \quad (12)$$

$$u_x = \frac{\int_V \rho_l u dV}{\int_V \rho_l dV} \quad (13)$$

where V is the computation domain, u is the velocity in x-axis, v is the velocity in y-axis and w is the velocity in z-axis for a unit mesh respectively. The characteristic time scale is $\tau_{ci}=(\rho_l r_0^3/\sigma)^{1/2}$. Based on u_{ci} and τ_{ci}, all velocities and time were non-dimensionalized as shown in Table 2.

Table 2. The dimensionless parameters

Non-dimensional jumping velocity	Non-dimensional X-axis velocity	Non-dimensional time scale
$u_{jump}^* = \frac{u_{jump}}{u_{ci}}$	$u_x^* = \frac{u_x}{u_{ci}}$	$t^* = \frac{t}{\tau_{ci}}$

During the merging of the droplets on the superhydrophobic surface, excess surface energy is converted into kinetic energy, which allows the droplet jumping from the surface. In this process, the conversion rate is very low (less than 6%) because surface energy is mostly dissipated by viscosity according to previous researches.[8, 30, 34] So, we also analyzed the surface energy and the kinetic energy. We can get the initial surface energy E_{surf} by equation $E_{surf}=\sigma A$, where A is the initial surface area of two droplets. When the two droplets are merging, we calculated the surface area by extracting the surface in software Tecplot360. As for the kinetic energy, we can get the jumping kinetic energy as $E_{kine}=mu_{jump}^2/2$.

3. Results and discussion

3.1 Numerical validation and morphological analysis

To validate our model, droplet jumping experiments were conducted. The experimental superhydrophobic surface, fabricated by the chemical deposition-etching method reported in our previous work,[47] has an apparent contact angle of 160.2±1.5°. A micropipettor was used to locate two small droplets on the superhydrophobic surface. After that, we produced tiny air current with the help of capillary tube, driving one droplet to move to another. Time-lapse images of the whole process were recorded by a high-speed camera.

Figure 2 shows the comparison of the droplet jumping process between the experimental result and the numerical one. In the experiments, the radius of left droplet is 736 μm, the right is 758 μm. Their ratio of radius is 0.97, so we can regard the droplets in the experiment as equal droplets. Five pictures before the droplet contact were selected and the average velocity during this period was calculated as the initial velocity of the moving droplet. The initial velocity of the left droplet in our experiment is 0.3 m/s. In the simulation, the initial velocity of the moving droplet is also set to 0.3 m/s.

As seen in Fig. 2, the variations of droplet morphologies from experiments and simulations correspond well which validates the correctness of our numerical method. At t^*=0, the moving droplet is in contact with the stationary droplet, then two droplets begin to merge. The merging process is accompanied with the expansion of the liquid bridge and the movement of the droplets. As shown in image at t^*=0.38, the liquid bridge is expanding. Since the left side droplet has an initial velocity, the shape of the liquid bridge is asymmetrical, and the deformation of the left part is faster (t^*=0.76). At t^*=1.53, the liquid bridge completes the expansion, but the droplet still oscillates in the horizontal direction asymmetrically, resulting in an asymmetrical droplet shape (t^*=1.90). Because the liquid bridge impinging on the substrate produces reaction force, the droplet moves upward and finally departs from substrate at t^*=3.81. After leaving the substrate, the droplet has both horizontal and vertical velocities, which indicates an oblique movement of the droplet.

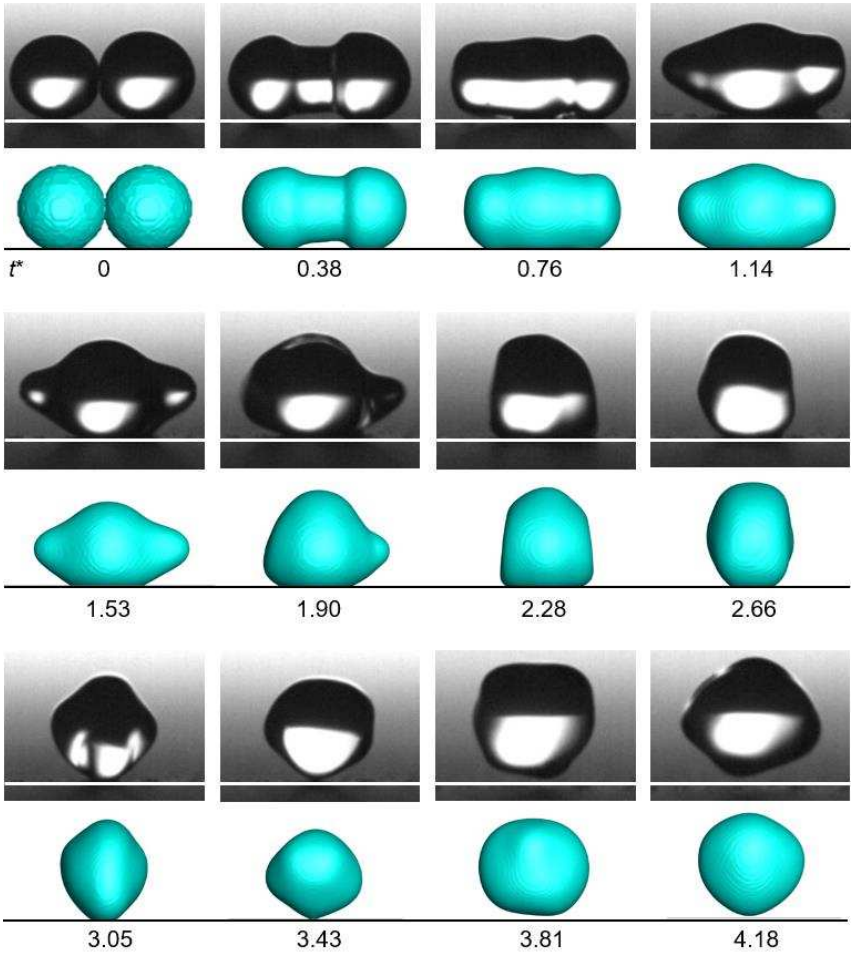

Fig. 2 Comparison of the droplet jumping process between experimental results and numerical one. For each row, the upper pictures are experimental results and the lower are simulation results. The initial velocity of the left droplet in the experiment is 0.3 m/s and the initial velocity of the left droplet in the simulation is set to 0.3 m/s. The dimensionless time is marked under the pictures in each row.

We also compared two simulation results with and without initial velocities to discuss the effects of initial velocities on droplet morphology (showed in Fig. 5). The initial velocity of the upper case is 0 m/s, lower is 0.5 m/s.

With the initial velocity input, the morphology evolution of the droplet is accelerated, and the degree of droplet asymmetry is increased. According to the simulation results, we demonstrated that the input of initial velocity accelerates liquid bridge expansion speed, leading the liquid bridge to impinge on the substrate earlier. In addition, as the initial velocity increases, the velocity of the coalescent droplet in the horizontal direction increases, which yields more displacement in horizontal direction. We will discuss more details about the velocity below.

3.2 Velocity analysis

Figure 3(a) shows the relationship between dimensionless jumping velocity and dimensionless time in the jumping process. Curves obtained at different initial velocities are distinguished by different symbols. In details, there are mainly two differences between the results of each curve. First, as the initial velocity increases, the time spend on the liquid bridge expansion and droplet shrinkage phases is significantly reduced. Before the two droplets are fully merged, the left droplet always has a relative velocity to the right, which accelerates the merging process. Second, the jumping velocity after droplet departure for each case is different. After the droplet leaves the surface, the curves of the first three results (V_0=0 m/s, 0.1 m/s, and 0.3 m/s) are close. But when the initial velocity increases to 0.5 m/s, the jumping velocity is significantly higher than the other cases. To explain this phenomenon, we counted the departure velocity, $V^*_{depar}=v_{depar}/u_{ci}$, and departure time, $t^*_{depar}=t_{depar}/\tau_{ci}$.

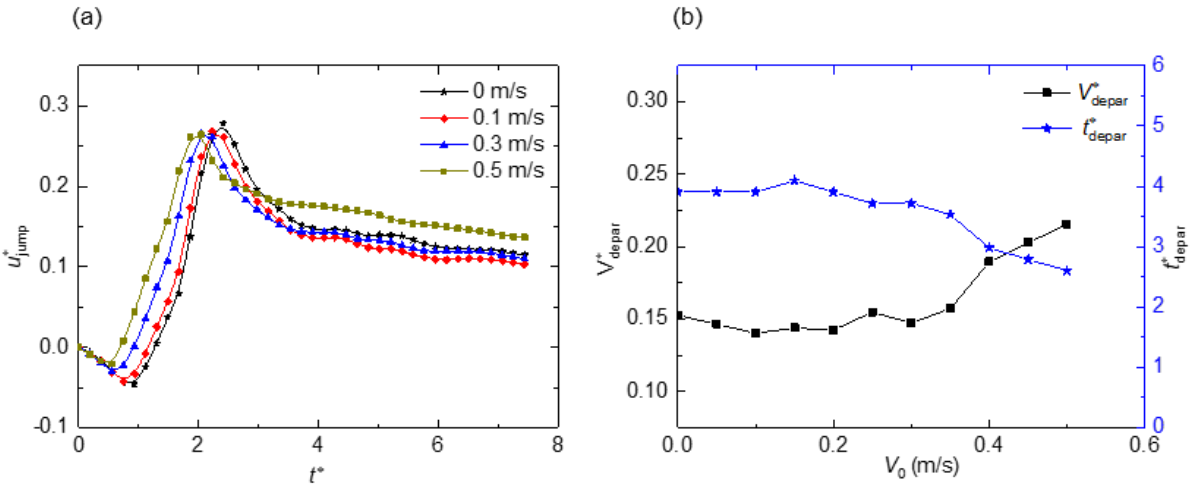

Fig.3 (a) Relationship between dimensionless jumping velocity and dimensionless time. The figure shows the tendency of the jumping speed under four different initial velocities: 0 m/s, 0.1 m/s, 0.3 m/s, 0.5 m/s, respectively. (b) Relationship between departure velocity and departure time with respect to various initial velocities. The y-axis parameters are dimensionless, and the x-axis unit is meter per second.

Figure 3(b) shows the relationship between departure velocity and departure time with respect to various initial velocities. In the beginning, when the initial velocity is little, the departure velocity in each case is very close. But after that, the departure velocities begin to increase with increasing initial velocities. The change trend of the

departure time is similar with that of the departure velocity. If considering the relationship between the departure velocity and the departure time, we can conclude that the two parameters are highly related. When the departure time is close, the departure velocity is also similar in same period. If the departure time is shortened, the departure velocity increases.

In order to explain the variation tendency of the departure velocity, we extracted the horizontal length of the droplet during the jumping process and defined the dimensionless length as L^*, $L^*=L/L_0$. Figure 4 shows the relationship between the dimensionless length and the dimensionless time. We chose three initial velocities, 0 m/s, 0.3 m/s, and 0.5 m/s as examples. From the results, the changing trend of the droplet length in the horizontal direction is similar regardless of the initial velocity. So, we explained the change of droplet length by taking V_0=0.5 m/s as an example and divided the whole jumping process into four stages according to the curve changing in Fig. 4. For easy understanding, we also provided the droplet morphology evolutions at each stage, as shown in Fig. 5. In stage a, droplets begin to merge, and the dimensionless length continues to reduce until the liquid bridge touches the substrate. Then, the droplet has a rapid expansion and the length increases. The second stage starts at t^*=1.02 when the droplet begins to shrink. The dimensionless length of the droplet decreases rapidly and until it reaches a local minimum at t^*=1.86. Then, stage c starts, during which the droplet oscillates slightly (first expands and then shrinks). We further divided the stage c into two parts, *i.e.* stage ci and stage cii. Stage ci is from t^*=1.86 to t^*=2.23; stage cii is from t^*=2.23 to t^*=2.60. The last part is stage d, when the droplet experiences a relative long-time expansion before next round oscillation in air. The stage demarcations are similar when the initial velocities are 0 m/s and 0.3 m/s, except that the demarcation times between stages are different.

We marked the departure points for three initial velocities in Fig. 4. As seen, the departure point is in stage ci when the initial velocity is 0.5 m/s, while for the other two cases (V_0=0 m/s and 0.3 m/s) the departure points are in stage d. Figure 5 also shows these results visually. From the above discussion, we have shown that the increasing in the initial velocity can accelerate the deformation of the droplet, so that the liquid bridge has a faster expansion velocity with a larger reaction force obtained from the substrate. But if the initial velocity is not large enough to help the droplet depart from the surface during expansion in stage ci, the droplet will enter stage cii and shrink again, and finally departs from the surface during the next expansion in stage d. Based on the simulation results, those droplets which can't depart in the stage ci finally depart from the surface in stage d. Departure at different stages result in different viscous dissipation. The earlier the departure time, the less the viscous dissipation before droplet departure, and the larger the jumping velocity.

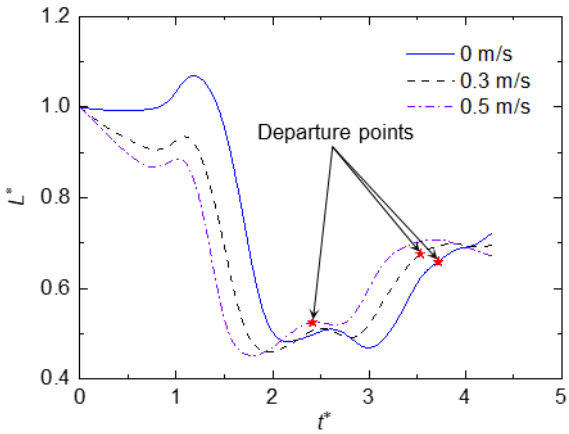

Fig. 4 Relationship between dimensionless horizontal length of droplets and dimensionless time under different initial velocities. The departure points for each case have marked on the figure.

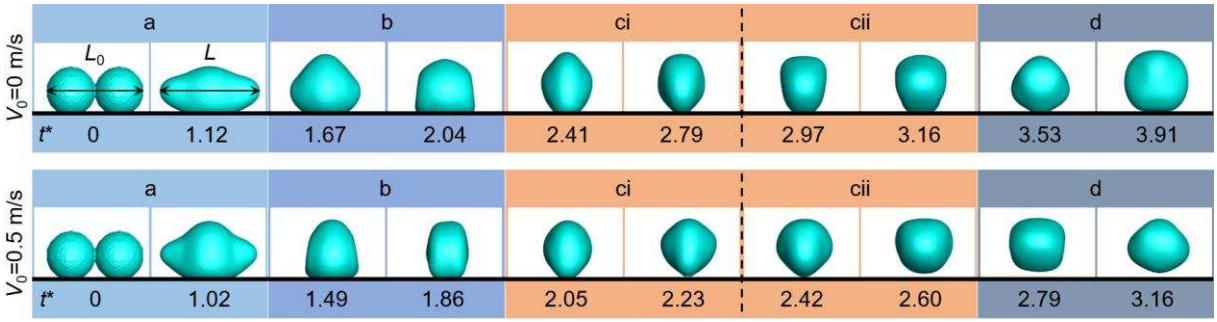

Fig. 5 Time-lapse images of the simulated droplet jumping. The initial velocity at the upper row is 0 m/s, the lower is 0.5 m/s, and the dimensionless time is marked under each row. Four stages are divided in the figure and distinguished in different background colors.

Figure 6 shows the droplet horizontal velocity variations during jumping with time. We selected three cases with different initial velocities to explain the variation of horizontal velocity. Three curves have the same trend. When the droplets begin to contact, there is a sharply drop in horizontal velocity during the initial phase of the curve. Subsequence, as the merging droplet oscillates on the substrate, the horizontal velocity of the droplet is fluctuant decreasing. After the droplet departs from the surface, the horizontal velocity decreases approximately linear.

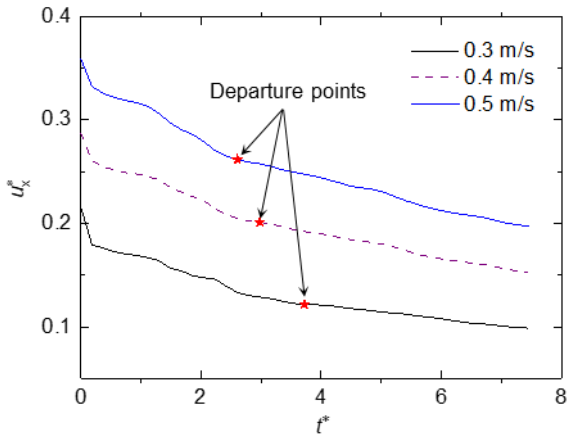

Fig. 6 Variations of dimensionless horizontal velocity with time during jumping under different initial velocities

3.3 Energy analysis

When two droplets merge into a large droplet, the surface area decreases which results in the decline of the surface energy. Reduced surface energy is converted into jumping kinetic energy, which allows the droplet to jump out from the surface. However, the conversion rate is very low, most of the energy is dissipated by the viscosity. According to previous researches, the conversion rate of the surface energy to the jumping kinetic energy is less than 6%.[8, 34] In this section, we discussed the energy conversion rates under these cases.

In section 2.2, we have defined the surface energy and the kinetic energy. Based on these discussions, we denoted the initial surface energy as $E_{surf,i}$, $E_{surf,i}=\sigma A_i$, the surface energy when the droplet departs from the surface as $E_{surf,d}$, $E_{surf,d}=\sigma A_d$,[38] where A_i is the initial surface area of two droplets and A_d is the surface area when the droplet departs from the surface. The energy conversion rate can be obtained according to the following formula.

$$\varepsilon=\frac{E_{kine}}{E_{surf,i}-E_{surf,d}} \quad (14)$$

We calculated the energy conversion rate according to Eq. (14). All the results are showed in Fig. 7 which marked as red points. To better show the trend, we plotted fit curve which is showed as black line. From the figure, when the initial velocity is 0 m/s, the conversion rate is 4.24%, this is corresponded to previous researches. At low initial velocity, the increasing in initial velocity has little effect on the energy conversion rate which is near 4%. But if the initial velocity continues to increase, the conversion rate shows a significant increase because the departure velocity and jumping velocity increase in these cases, as discussed in section 3.2.

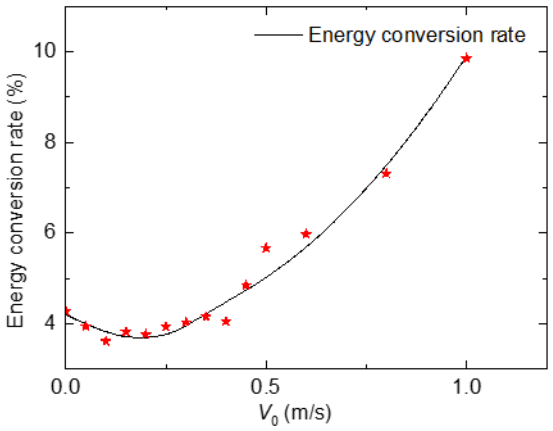

Fig. 7 Relationship between energy conversion rate and initial velocity. Red points are simulation results, and the black line is fit curve.

4. Conclusions

In summary, we used the VOF method with a dynamic contact angle model to investigate the droplet jumping phenomenon induced by the coalescence of a static droplet and a moving one with different initial velocities. The

simulation results showed good agreement with the experimental results. We analyzed the droplet morphology evolution, velocity variation and energy conversion rate during the jumping process, and revealed the differences to that of static droplets. The main conclusions are summarized in below.

(i) The droplet morphology evolution during jumping induced by the coalescence of a moving droplet and a static one is similar to that of static droplets, except that the initial velocity of the moving droplet promotes the liquid bridge expansion, and accelerates the droplet deformation, leading to the droplet shape asymmetry.

(ii) For the droplet jumping induced by the coalescence of a moving droplet and a static one, the departure velocity is similar at small initial velocity of the moving droplet. With further increasing of the initial velocity, *i.e.*, >0.5 m/s, the droplet departure velocity becomes significantly larger due to the departure at an earlier stage of the morphology evolution (stage cii).

(iii) At small initial velocities of the moving droplet, the conversion rate from the surface energy to jumping kinetic energy changes slightly. However, as the initial velocity is larger than a critical value, the conversion rate is positively correlated with the initial velocity, and even exceeds the boundary of 6%.

Acknowledgement

This work is supported by the National Postdoctoral Program for Innovative Talents (No. BX20180024), the China Postdoctoral Science Foundation (No. 2019M650444), and the National Natural Science Foundation of China (No. 11772034).

Conflict of interest statement

We declare no any interest conflict.

References

1. J. B. Boreyko and C. H. Chen, Phys. Rev. Lett., 2009, 103, 184501.
2. G. S. Watson, M. Gellender and J. A. Watson, Biofouling, 2014, 30, 427-434.
3. X. Yan, L. Zhang, S. Sett, L. Feng, C. Zhao, Z. Huang, H. Vahabi, A. K. Kota, F. Chen and N. Miljkovic, ACS Nano, 2019, 13, 1309-1323.
4. M. D. Mulroe, B. R. Srijanto, S. F. Ahmadi, C. P. Collier and J. B. Boreyko, ACS Nano, 2017, 11, 8499-8510.
5. H. Vahabi, W. Wang, S. Davies, J. M. Mabry and A. K. Kota, ACS Appl. Mater. Interfaces, 2017, 9, 29328-29336.
6. F. Chu, X. Wu, B. Zhu and X. Zhang, Appl. Phys. Lett., 2016, 108, 194103.
7. H. Cha, C. Y. Xu, J. Sotelo, J. M. Chun, Y. Yokoyama, R. Enright and N. Miljkovic, Phys. Rev. Fluids, 2016, 1, 064102.

8. F. J. Liu, G. Ghigliotti, J. J. Feng and C. H. Chen, J. Fluid Mech., 2014, 752, 39-65.
9. Y. P. Cheng, J. L. Xu and Y. Sui, Int. J. Heat Mass Transfer, 2016, 95, 506-516.
10. Y. Chen and Y. Lian, Phys. Fluids, 2018, 30, 112102.
11. Z. Yuan, R. Wu and X. Wu, Int. J. Heat Mass Transfer, 2019, 135, 345-353.
12. X. Liu, P. Cheng and X. Quan, Int. J. Heat Mass Transfer, 2014, 73, 195-200.
13. X. Liu and P. Cheng, Int. Commun. Heat Mass Transfer, 2015, 64, 7-13.
14. R. Enright, N. Miljkovic, J. Sprittles, K. Nolan, R. Mitchell and E. N. Wang, ACS Nano, 2014, 8, 10352-10362.
15. J. B. Boreyko, Y. Zhao and C.-H. Chen, Appl. Phys. Lett., 2011, 99, 234105.
16. J. Oh, P. Birbarah, T. Foulkes, S. L. Yin, M. Rentauskas, J. Neely, R. C. N. Pilawa-Podgurski and N. Miljkovic, Appl. Phys. Lett., 2017, 110, 123107.
17. K. F. Wiedenheft, H. A. Guo, X. P. Qu, J. B. Boreyko, F. J. Liu, K. G. Zhang, F. Eid, A. Choudhury, Z. H. Li and C. H. Chen, Appl. Phys. Lett., 2017, 110, 141601.
18. B. Traipattanakul, C. Y. Tso and C. Y. H. Chao, Int. J. Heat Mass Transfer, 2019, 135, 294-304.
19. K. M. Wisdom, J. A. Watson, X. P. Qu, F. J. Liu, G. S. Watson and C. H. Chen, Proc. Natl. Acad. Sci. U. S. A, 2013, 110, 7992-7997.
20. C. Dietz, K. Rykaczewski, A. G. Fedorov and Y. Joshi, Appl. Phys. Lett., 2010, 97, 033104.
21. N. Miljkovic, R. Enright, Y. Nam, K. Lopez, N. Dou, J. Sack and E. N. Wang, Nano Lett., 2013, 13, 179-187.
22. F. Chu, X. Wu and L. Wang, ACS Appl. Mater. Interfaces, 2018, 10, 1415-1421.
23. Q. Zhang, M. He, J. Chen, J. Wang, Y. Song and L. Jiang, Chem. Commun., 2013, 49, 4516-4518.
24. J. B. Boreyko and C. P. Collier, ACS Nano, 2013, 7, 1618-1627.
25. F. Chu, D. Wen and X. Wu, Langmuir, 2018, 34, 14562-14569.
26. Y. Shen, M. Jin, X. Wu, J. Tao, X. Luo, H. Chen, Y. Lu and Y. Xie, Appl. Therm. Eng., 2019, 156, 111-118.
27. F.-C. Wang, F. Yang and Y.-P. Zhao, Appl. Phys. Lett., 2011, 98, 053112.
28. T. Mouterde, T.-V. Nguyen, H. Takahashi, C. Clanet, I. Shimoyama and D. Quéré, Phys. Rev. Fluids, 2017, 2, 112001.
29. P. Lecointre, T. Mouterde, A. Checco, C. T. Black, A. Rahman, C. Clanet and D. Quéré, Phys. Rev. Fluids, 2019, 4, 013601.
30. F. Liu, G. Ghigliotti, J. J. Feng and C.-H. Chen, J. Fluid Mech., 2014, 752, 22-38.
31. Y. Nam, H. Kim and S. Shin, Appl. Phys. Lett., 2013, 103, 161601.
32. K. Wang, R. X. Li, Q. Q. Liang, R. Jiang, Y. Zheng, Z. Lan and X. H. Ma, Appl. Phys. Lett., 2017, 111, 061603.
33. J. Wasserfall, P. Figueiredo, R. Kneer, W. Rohlfs and P. Pischke, Phys. Rev. Fluids, 2017, 2, 123601.

34. F. Chu, Z. Yuan, X. Zhang and X. Wu, Int. J. Heat Mass Transfer, 2018, 121, 315-320.
35. K. Wang, Q. Q. Liang, R. Jiang, Y. Zheng, Z. Lan and X. H. Ma, Langmuir, 2017, 33, 6258-6268.
36. R. Attarzadeh and A. Dolatabadi, Phys. Fluids, 2017, 29, 012104.
37. K. Wang, Q. Liang, R. Jiang, Y. Zheng, Z. Lan and X. Ma, RSC Adv., 2016, 6, 99314-99321.
38. H. Vahabi, W. Wang, J. M. Mabry and A. K. Kota, Sci. Adv., 2018, 4, euaa3488.
39. H. G. Weller, G. Tabor, H. Jasak and C. Fureby, Comput. Phys., 1998, 12, 620-631.
40. J. Zhang, M. K. Borg and J. M. Reese, Int. J. Heat Mass Transfer, 2017, 115, 886-896.
41. M. Renardy, Y. Renardy and J. Li, J. Comput. Phys., 2001, 171, 243-263.
42. N. Nikolopoulos, A. Theodorakakos and G. Bergeles, Int. J. Heat Mass Transfer, 2007, 50, 303-319.
43. S. F. Kistler, “Hydrodynamics of wetting,” in Wettability, edited by J. C. Berg (Marcel Dekker, New York, 1993), 311.
44. I. V. Roisman, L. Opfer, C. Tropea, M. Raessi, J. Mostaghimi and S. Chandra, Colloids Surf., A, 2008, 322, 183-191.
45. I. Malgarinos, N. Nikolopoulos, M. Marengo, C. Antonini and M. Gavaises, Adv. Colloid Interface Sci., 2014, 212, 1-20.
46. S. Afkhami, S. Zaleski and M. Bussmann, J. Comput. Phys., 2009, 228, 5370-5389.
47. F. Chu and X. Wu, Appl. Surf. Sci., 2016, 371, 322-328.